Supplementary Materials

Computational methods and the crystallographic data of the KCuS

We used density functional theory to calculate the ground state of KCuS with a *Pnma* structure and the GGA-PBE[S1] formalism for the exchange-correlation functional. We used the projector augmented-wave method for the interactions between ions and valence electrons and set the energy cutoff to 600 eV. We used a Γ-centered *k*-mesh of 5×5×5 for BZ sampling. We performed the lattice dynamic calculations to obtain the phonon dispersion of KCuS at its equilibrium lattice constants in the PHONOPY package[S2] using density functional perturbation theory. We simulated the topological behaviors of the [100], [010], and [001] phonon surface states by constructing lattice models based on KCuS.

The crystallographic data of the KCuS with a *Pnma*-type is obtained from the Materials Project database[S3]. Figs. S1(a) and S1(b) show the crystal structure of KCuS with a *Pnma*-type structure under different view sides. In one unit cell, KCuS contains 12 atoms (i.e., four Cu, four K, and four S atoms located at the 4a (0.0, 0.5, 0.0), 4c (0.84639, 0.75, 0.52184), and 4c (0.41155, 0.25, 0.72286) Wyckoff positions, respectively). The lattice constants of KCuS are obtained using first-principles calculations, and the values are a = 10.726 Å, b = 5.3087 Å, and c = 6.348 Å, respectively, agreeing well with values in Materials Project database[S3] (a = 10.716 Å, b = 5.315 Å, and c = 6.299 Å). Although the KCuS is a theoretically proposed compound, its formation energy, elastic constants, and the phonon dispersion exhibited in Ref. [S3] clearly demonstrated the stability of KCuS. For *Pnma*-type KCuS, its symmetry operators are summarized as follows: two screw rotations $\widetilde{C_{2z}} = \left\{C_{2z}\middle|\frac{1}{2}0\frac{1}{2}\right\}$ and $\widetilde{C_{2y}} = \left\{C_{2y}\middle|0\frac{1}{2}0\right\}$, a spatial inversion $\mathcal{P}$, and time-reversal symmetry $\mathcal{T}$ with $\mathcal{T}^2 = 1$ (since it is a spinless system).

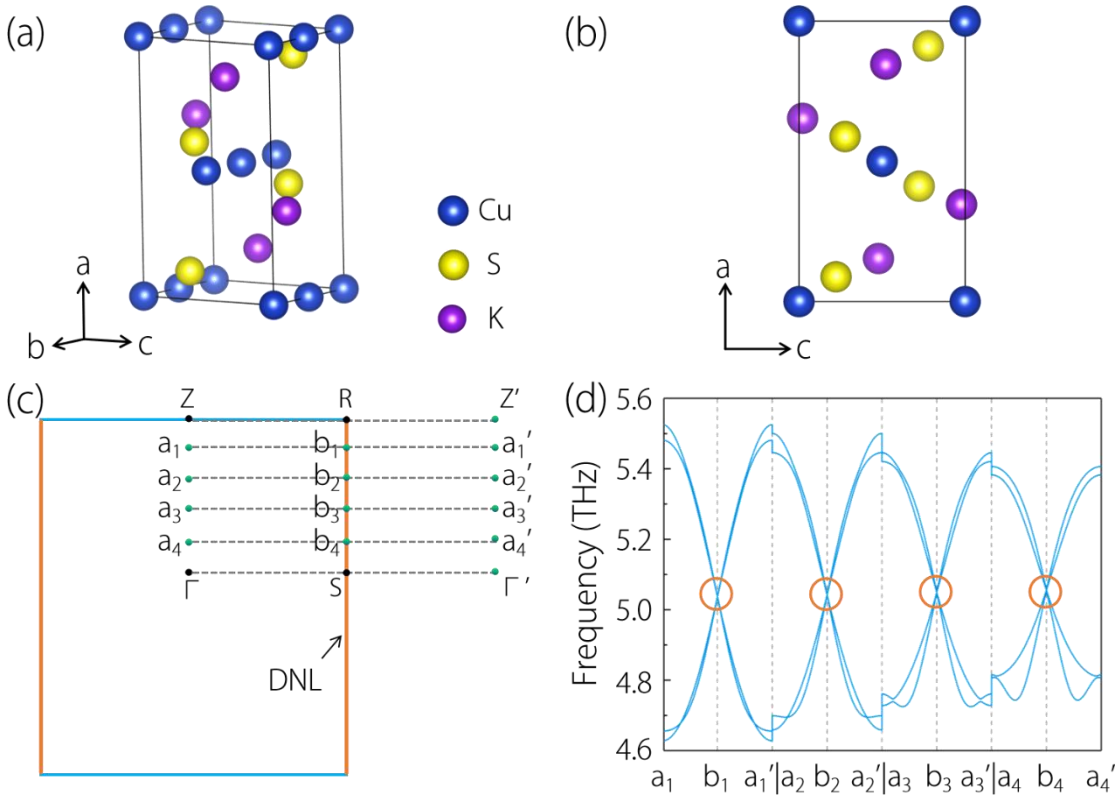

FIG. S1. (a) and (b) crystal structures of KCuS with a *Pnma*-type structures under different viewsides. (c) Some selected symmetry points in the $[1\bar{1}0]$ plane. (d) Calculated phonon dispersions along the a_1-b_1-a_1', a_2-b_2-a_2', a_3-b_3-b_3', and a_4-b_4-a_4' paths, where the linear phonon band crossing points are marked with orange circles.

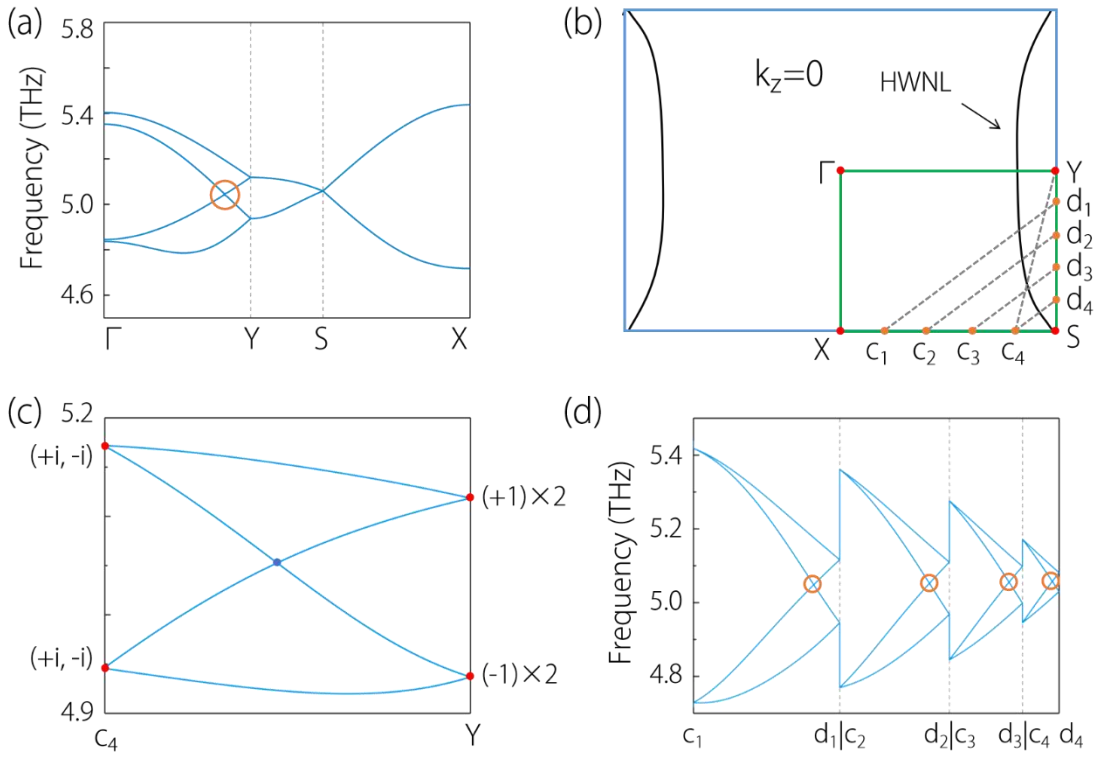

FIG. S2. (a) Enlarged phonon dispersion of the *Pnma*-type KCuS in R3 region of Fig. 2(b) where the neck crossing-point of the hourglass-like dispersion along the Γ-Y path is marked with circle. (b) Shape of the HWNL and a series of selected symmetry points in the $k_z = 0$ plane. (c) Schematic of hourglass dispersion along the c_4-Y direction. (d) Detailed phonon dispersions along the c_m-d_m (m = 1, 2, 3, 4) paths where the neck crossing-points of the hourglass dispersions are marked with orange circles.

DNL and HWNL phonons coexist in some realistic material samples with *Pnma* type structure

The minimum symmetry requirements for HWNL are the presence of glide mirror and an antiunitary operation. We take the one on k_z plane as an example, if there is a glide mirror $\left\{\widetilde{M}_z\middle|\frac{a}{2}\frac{b}{2}\right\}$, (at least, one of them is nonzero, with a+b=1). Then, it shows that, if a=1, b=0, $\widetilde{M}_z^2 = e^{-ik_x}$, and $g_z = \pm e^{-ik_z}$. Along its invariant space, the antiunitary makes $|g_z = 1(-1)\rangle$ degenerate at where $k_x = 0$, and $|g_z = i\rangle$ and $|g_z = -i\rangle$ degenerate at $k_x = \pi$. Hence, there must be a band switching, leading to an hourglass node point. Due to it is on the invariant of glide mirror, such a point cannot be isolated, thus forming a nodal line. In contrast, for the Dirac point, besides the above symmetry, it also requires a spatial symmetry which anticommutes with $\widetilde{M}_z$, double the

degeneracy. To be noted, for Dirac point, $\widetilde{M}_z$ is not necessary, it can be screw rotation. Therefore, in the symmetry aspect, the presence of HWNL not usually implies the presence of nodal point.

However, space group 62 satisfies the above-mentioned symmetry conditions for the existence of WNL and DNL. Therefore, WNL and DNL can coexist in materials with SG No. 62. Note that KCuS is a theoretically proposed compound, and in this Letter, we also find some realistic materials (with a *Pnma* -type structure) as the hosts with the DNL and HWNL phonons.

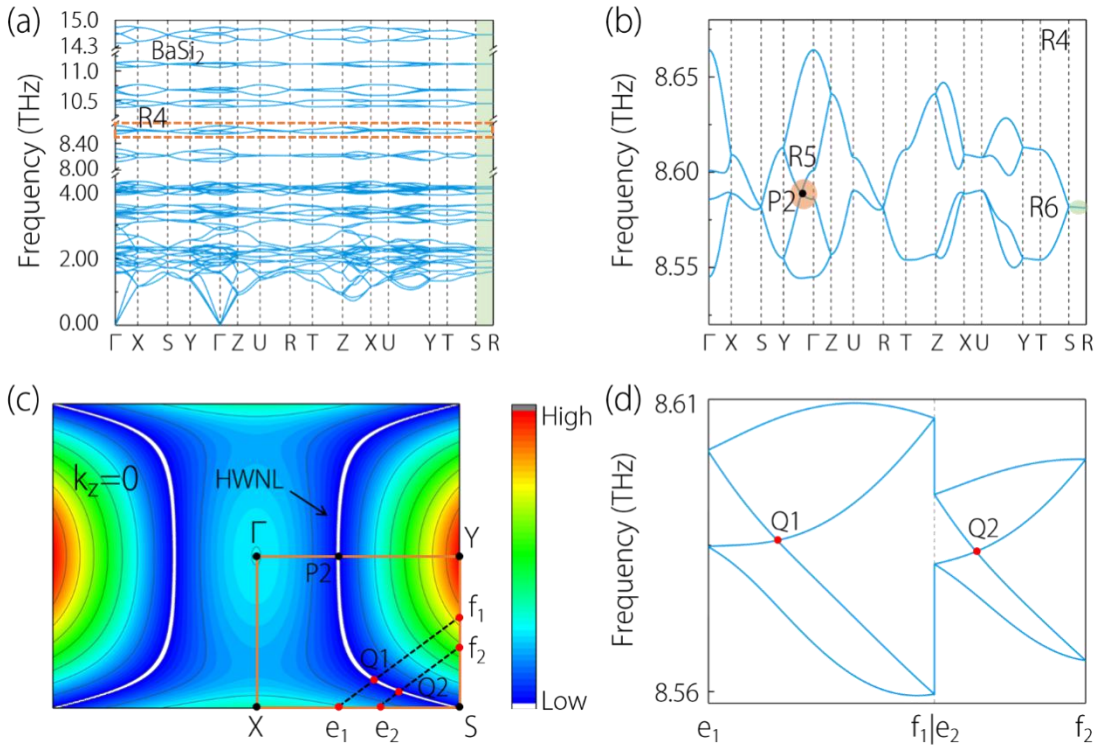

FIG. S3. (a) Phonon dispersion of $BaSi_2$ along the $\Gamma-X-S-Y-\Gamma-Z-U-R-T-Z-X-U-Y-T-S-R$ paths and (b) enlarged figure of R4 region in (a). The phonon band crossing point P2 on the $Y-\Gamma$ (in region R5). The DNL in region R6 along S-R path is highlighted with green color. (c) The shape of HWNL in the $k_z=0$ plane from DFT calculation. The white color denotes the lack of gap between the two phononic bands in the $k_z=0$ plane, i.e., we use the white line to indicate the HWNL in this plane. (d) The phonon dispersions along the e_1 (0.5, 0.2, 0.0)-f_1 (0.2, 0.5, 0.0) and e_2 (0.5, 0.3, 0.0)-f_2 (0.3, 0.5, 0.0) paths. Hourglass dispersions appear along the e_1-f_1 and e_2-f_2 paths and the Q1 and Q2 are the neck points of the hourglass.

The first example is $BaSi_2$. The $BaSi_2$ with an orthorhombic structure is a stable form at atmospheric pressure and room temperature[S4, S5]. The phonon dispersion of $BaSi_2$ along the $\Gamma-X-S-Y-\Gamma-Z-U-R-T-Z-X-U-Y-T-S-R$ paths are given in Fig. S3(a). It

is clear that the phonon bands in region R4 are well separated from other phonon bands in other frequencies. The enlarged figures of region R4 are shown in Fig. S3(b). From Fig. S3(b), a phonon band crossing point P2 in region R5 and DNL phonons along S-R path in region R6 are obvious. As shown in Fig. S3(c), one can see that the P2 point belongs to a WNL (see the white line) in the $k_z = 0$ plane. Moreover, all the points of the WNL are the neck points of the hourglass dispersions (see the examples of Q1 and Q2 points as shown in Fig. S3(d)). Hence, the WNL plotted in Fig. S3(c) should be HWNL.

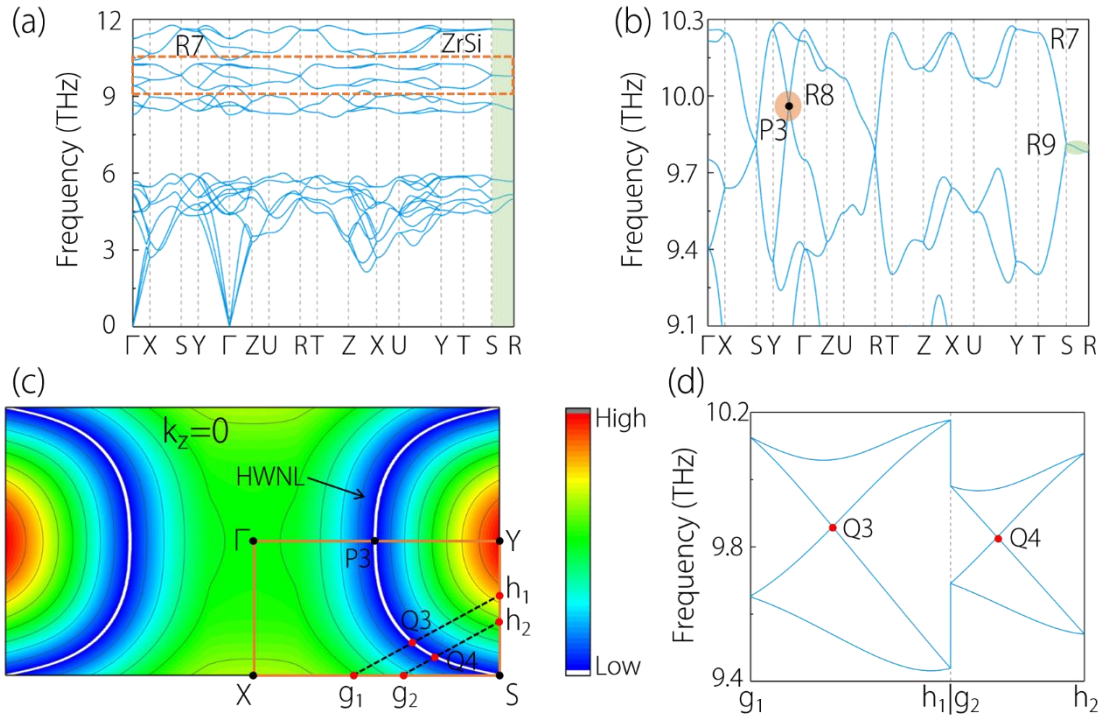

FIG. S4. (a) Phonon dispersion of ZrSi along *the* Γ − X − S − Y − Γ − Z − U − R − T − Z − X − U − Y − T − S − R paths and (b) enlarged figure of R7 region in (a). The phonon band crossing point on the Y − Γ (in region R8) is named as P3. The DNL in region R9 along *S*-*R* path is highlighted with green color. (c) The shape of HWNL in the $k_z = 0$ plane from DFT calculation. We use the white line to indicate the HWNL in $k_z = 0$ plane. (d) The phonon dispersions along the g_1 (0.5, 0.2, 0.0)-h_1 (0.2, 0.5, 0.0) and g_2 (0.5, 0.3, 0.0)-h_2 (0.3, 0.5, 0.0) paths. The Q3 and Q4 points are the neck crossing-points of the hourglass-type dispersions, along the g_1-h_1 and g_2-h_2, respectively.

The second example is ZrSi compound. Brewer and Krikorian[S6] showed that ZrSi is with an orthorhombic FeB-type structure. The phonon dispersion of ZrSi along the $\Gamma - X - S - Y - \Gamma - Z - U - R - T - Z - X - U - Y - T - S - R$ paths is given in Fig. S4(a). The enlarged figure of

the phonon bands in region R7 is shown in Fig. S4(b). Obviously, DNL phonons along S-R path (see region R9 in Fig. S4(b)) and a phonon band-crossing point P3 (see region R8 in Fig. S4(b)) can be observed. The point P3 belongs to a HWNL in the $k_z = 0$ plane (see Fig. S4(c)). To further prove the WNL in the $k_z = 0$ plane is HWNL, we exhibit the phonon dispersions of ZrSi along the g_1-h_1 and g_2-h_2 paths in Fig. S4(d)). One finds that the points Q3 and Q4 are the neck points of the hourglass dispersions along the g_1-h_1 and g_2-h_2 paths and the WNL is formed by the neck points (such as P3, Q3, and Q4) of the hourglass dispersions.

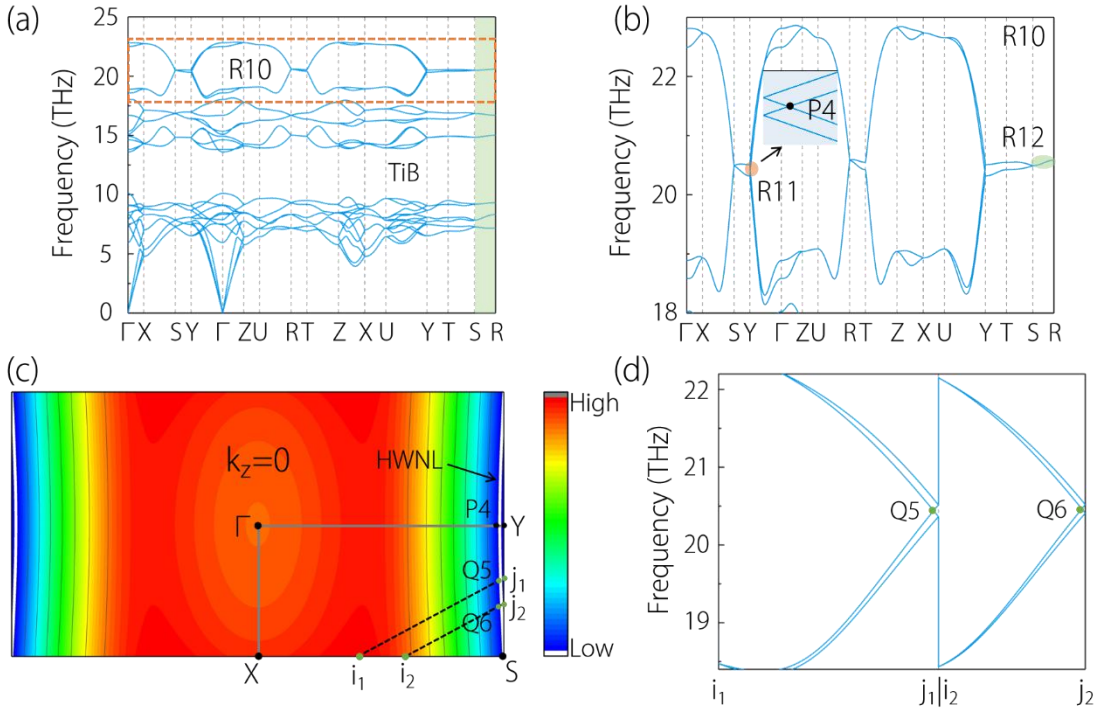

FIG. S5. (a) Phonon dispersion of TiB along the $\Gamma - X - S - Y - \Gamma - Z - U - R - T - Z - X - U - Y - T - S - R$ paths and (b) enlarged figure of R10 region in (a). The phonon band crossing point on $Y - \Gamma$ (in region R11) is named as P4. The DNL in region R12 along S-R path is highlighted with green color. (c) The shape of HWNL (see white line) in the $k_z = 0$ plane from DFT calculation. (d) The phonon dispersions along the i_1 (0.5, 0.2, 0.0)-j_1 (0.2, 0.5, 0.0) and i_2 (0.5, 0.3, 0.0)-j_2 (0.3, 0.5, 0.0) paths. The Q5 and Q6 points are the neck crossing-points of the hourglass dispersions, along i_1-j_1 and i_2-j_2, respectively.

The final example is TiB and it has been prepared by arc-melting a mixture of powdered boron and titanium of high purity[S7]. The structure of TiB has been determined by Decker and Kasper[S7] via the single-crystal and powder methods. They proved that TiB is with the

FeB-type structure and with space group number 62. The phonon dispersion of TiB along the paths $\Gamma - X - S - Y - \Gamma - Z - U - R - T - Z - X - U - Y - T - S - R$ is given in Fig. S5(a). The region R10 in Fig. S5(a) is of our interest. The enlarged figure of the phonon bands in region R10 is shown in Fig. S5(b). Two interesting types of phonon band features can be observed: (i) the phonon bands are four-fold degenerate along the S-R (see the region R12 in Fig. S5(b)); (ii) hourglass dispersions appear along the $Y - \Gamma$ (see the region R11 in Fig. S5(b)). The neck point, P4, of the hourglass is a crossing-point with two-fold degeneracy. As shown in Fig. S5(c), we show that the P4 belongs to HWNL. For clarity, the hourglass dispersions along the i_1-j_1 and i_2-j_2 paths, and the two neck points, Q5 and Q6, of the hourglass dispersions are also exhibited in Fig. S5(d).

As shown in Fig. S3(a), Fig. S4(a) and Fig. S5(a), the phonon bands in regions R4, R7, and R10 are well separated from other optical branches, reflecting that the DNL and HWNL phonons are "clean" and may be easily detected by some experimental techniques, such as infrared spectroscopy[S8], x-ray scattering[S9], and inelastic neutron scattering[S10].

References

[S1] J. P. Perdew, K. Burke, and M. Ernzerhof, Phys. Rev. Lett. **80**, 891 (1998).

[S2] A. Togo and I. Tanaka, Scr. Mater. **108**, 1 (2015).

[S3] https://www.materialsproject.org/materials/mp-28270/

[S4] H. Schhfer, K. H. Janzon, and A. Weiss, Angew. Chem. Int. Ed. Engl. **2**, 393 (1963).

[S5] K.H. Janzon, H. Schäfer, and A. Weiss, Z. Anorg. Allg. Chem. **372**, 87 (1970).

[S6] L. Brewer and O. Krikorian, USAEC, UCRL-2544 (1954).

[S7] B. F. Decker and J. S. Kasper, Acta Crystallogr. **7**, 77 (1954).

[S8] I.-H. Lee, D. Yoo, P. Avouris, T. Low, and S.-H. Oh, Nat. Nanotechnol. **14**, 313 (2019).

[S9] M. Mohr, J. Maultzsch, E. Dobardžić, S. Reich, I. Milošević, M. Damnjanović, A. Bosak, M. Krisch, and C. Thomsen, Phys. Rev. B **76**, 035439 (2007).

[S10] O. Delaire, J. Ma, K. Marty, A. F. May, M. A. McGuire, M. H. Du, D. J. Singh, A. Podlesnyak, G. Ehlers, M. D. Lumsden, and B. C. Sales, Nat. Mater. **10**, 614 (2011).